ACS APPLIED MATERIALS & INTERFACES



Article

# Low Frequency Noise in Layered ReS Field Effect Transistors on HfO and its Application for pH Sensing

Wugang Liao, Wei Wei, Yu Tong, Wai Kin Chim, and Chunxiang Zhu

*ACS Appl. Mater. Interfaces*, **Just Accepted Manuscript** • DOI: 10.1021/acsami.8b00193 • Publication Date (Web): 01 Feb 2018



ACS Publications

ACS Applied Materials & Interfaces is published by the American Chemical Society. 1155 Sixteenth Street N.W., Washington, DC 20036

# Low Frequency Noise in Layered $ReS_2$ Field Effect Transistors on $HfO_2$ and its Application for pH Sensing

*Wugang Liao*[†,‡], *Wei Wei*[†,‡], *Yu Tong*[†,‡], *Wai Kin Chim*[†], *and Chunxiang Zhu*[†,‡,*]

[†]Department of Electrical and Computer Engineering,

National University of Singapore, 4 Engineering Drive 3, 117583 Singapore

[‡]Centre for Advanced 2D Materials and Graphene Research Centre, National University of Singapore, 6 Science Drive 2, 117546 Singapore

KEYWORDS: 2D material, rhenium disulfide, low-frequency noise, pH sensing, detection limit

[*]E-mail address: elezhucx@nus.edu.sg (C. Zhu)

**Abstract:**

Layered rhenium disulfide ($ReS_2$) field effect transistors (FETs), with thickness ranging from few to dozens of layers, are demonstrated on 20 nm-thick $HfO_2$/Si substrates. A small threshold voltage of -0.25 V, high on/off current ratio of up to ~$10^7$, small subthreshold swing of 116 mV/dec, and electron carrier mobility of 6.02 $cm^2/V \cdot s$ are obtained for the two-layer $ReS_2$ FETs. Low frequency noise characteristics in $ReS_2$ FETs are analyzed for the first time and it is found that the carrier number fluctuation mechanism well describes the flicker (1/*f*) noise of $ReS_2$ FETs with different thicknesses. pH sensing using two-layer $ReS_2$ FET with $HfO_2$ as sensing oxide is then demonstrated with a voltage sensitivity of 54.8 mV/pH and a current sensitivity of 126. The noise characteristics of the $ReS_2$ FET based pH sensors are also examined and a corresponding detection limit of 0.0132 pH is obtained. Our studies suggest the high potential of $ReS_2$ for future low-power nanoelectronics and biosensor applications.

## 1. Introduction

During the past decade, triggered by the exciting properties of graphene,[1] two-dimensional (2D) transition metal dichalcogenides (TMDs) have emerged as potential candidate materials for future digital electronics, optoelectronics and sensing applications.[2-4] Molybdenum- and tungsten-based TMDs, such as molybdenum disulfide ($MoS_2$) and tungsten diselenide ($WSe_2$), are among the most intensively investigated.[5-11] Very recently, rhenium disulfide ($ReS_2$), as a new member of TMDs, has gained considerable attention owing to its promising applications for logic circuits,[12] anisotropic electronics[13-15] and sensors.[16-18] Different from the conventional structure of $MoS_2$ and $WSe_2$ *etc*, $ReS_2$ has a unique distorted octahedral (1T) crystal structure with triclinic symmetry, which results in much weaker interlayer coupling.[19, 20] Many demonstrations have been reported ranging from the material synthesis to transistors and photodetectors, such as chemical vapor deposition synthesized

$ReS_2$ on large-area substrate,[21] high mobility of up to 1100 $cm^2/V \cdot s$ at 4 K for ionic liquid gated $ReS_2$ field effect transistor (FET),[22] and high photoresponsivity of $2.5 \times 10^7$ $A \cdot W^{-1}$ in exfoliated thick $ReS_2$ photodetector.[16] These encouraging results suggest that $ReS_2$ could be a very promising candidate for future nanoelectronics. However, in most demonstrations, FETs were fabricated on a thick silicon dioxide ($SiO_2$) (with 90 nm or 285 nm thickness) coated on highly doped silicon (Si). Although this favors thickness identification of 2D flakes, due to strong optical contrast, it results in poor gate controllability with subthreshold swings (*SS*) of the FETs usually larger than 1 V/dec. A high *SS* leads to a large driving voltage and high power consumption, and thus a small *SS* in 2D FETs is highly desired. Introducing a thin high dielectric constant (high-$k$) dielectric, such as $HfO_2$ and $Al_2O_3$, to replace the thick $SiO_2$ is conducive to the scaling down of the gate dielectric thickness and is a promising solution for small *SS* and low voltage operation.[23] Very recently, Xu *et al.*[24] reported a gate structure of $Al_2O_3$ (25 nm)/ITO(70 nm)/$SiO_2$ (200 nm)/Si to achieve both good optical identification of 2D materials and excellent gate controllability with reported *SS* below 100 mV/dec. Nevertheless, such a method suffers from the processing complexity.

In addition, low frequency noise (LFN) is another key limiting factor to the performance of nanoelectronics[25-27] and this becomes more pronounced in miniaturized devices operated under low voltages, such as carbon nanotubes,[28] Si nanowire FETs,[29] graphene FETs,[30] and atomic-layer TMD transistors.[26, 31-34] The study of LFN is widely considered as a versatile method in providing the characteristics of traps in the gate stack and their charge dynamics,[35] and a low LFN is highly desirable for a large margin in nanoscale devices. As for sensor applications, where 2D materials may have strong potentials owing to their high surface-to-volume ratio,[36] a small LFN is necessitated to achieve a high detection resolution. LFN in 2D materials such as graphene FETs[35, 37] and Mo- and W-based TMDs FETs[27, 32, 33, 38, 39] have been extensively investigated, and different dominant mechanism (i.e., carrier mobility fluctuation, carrier number fluctuation, and their combination) have been reported in 2D FETs depending on their materials, fabrication process and environments. However, an exploration of the LFN in the fascinating $ReS_2$ FETs is still lacking. In this article, we demonstrate $ReS_2$ FETs fabricated on 20 nm-thick $HfO_2$ on Si substrate, exhibiting a small threshold voltage of -0.25 V, high on/off current ratio of up to ~ $10^7$, low *SS* of 116 mV/dec and electron mobility of 6.02 $cm^2$/Vs. pH sensing using $ReS_2$ FETs are also demonstrated using $HfO_2$ sensing layer with a sensitivity of 54.8 mV/dec. LFN in $ReS_2$ FETs, in dry and pH sensing wet environment, are both characterized for the first time, and a detection limit of 0.0132 pH is achieved.

## 2. Results and Discussion

**Electrical Characteristics of the $ReS_2$ FETs.** To probe the electrical performances and LFN characteristics, we prepared $ReS_2$ FETs which is depicted in **Figure 1**a. Highly doped p++ Si substrates (as back gate) were coated with 20 nm-thick $HfO_2$ deposited by atomic layer deposition (ALD). The $HfO_2$ by ALD has a smooth surface with a mean roughness of ~0.3 nm, which is confirmed by atomic force microscopy (AFM) [Figure S1]. The capacitance density of 20 nm-thick $HfO_2$ was determined to be 6.7 × $10^{-7}$ F/$cm^2$ (Figure S2) and a dielectric constant (*k*) of 15.4 was extracted. It should be noted that although the 20 nm-thick $HfO_2$ on Si provides slightly weaker optical contrast for few-layer $ReS_2$ flakes, as compared to 285 nm-thick $SiO_2$ nm, it can still be identifiable (Figure S3). Figure 1b shows an optical image of a pair of Cr/Au electrodes deposited on a $ReS_2$ flake. The thickness of the $ReS_2$ flake measured by AFM is about 1.4 nm (shown in Figures 1c and 1d), corresponding to two atomic layers. Figure 1e shows the Raman spectrum of the two-layer $ReS_2$ flake. Two main Raman peaks located at 150 and 210.5 $cm^{-1}$ are observed, which correspond to the in-plane ($E_{2g}$) and mostly out-of plane ($A_{1g}$) vibrational modes of $ReS_2$, respectively.[40, 41] The Raman peaks appeared at 160 and 233.6 $cm^{-1}$ are attributed to the in-plane vibrational mode for Re atoms while the peaks observed at 131.5 and 305.6 $cm^{-1}$ are attributed to the out-of plane vibrational mode for Re atoms and the in-plane vibrational mode for S atoms. The series of Raman modes observed in the range of 100 - 400 $cm^{-1}$ are in good agreement with the literature.[42, 43] The Raman spectra of $ReS_2$ flakes with different thicknesses are similar to the two-layer $ReS_2$, which are shown in Figure S4.

Output curves and transfer characteristics for the two-layer (1.4 nm-thick) $ReS_2$ FET are depicted in **Figures 2**a - 2d. A typical n-type transport for $ReS_2$ FETs is observed. The linear and symmetric drain current vs drain voltage ($I_{DS}$-$V_{DS}$) curves at low drain voltage from -0.2 to 0.2 V presented in Figure 2a indicate an ohmic contact between Cr/Au and $ReS_2$ channel. The contact resistance between Cr/Au contacts and our two-layer $ReS_2$ is extracted to be 7.21 kΩ·μm based on the Y-function method,[44, 45] which is similar to that reported in $ReS_2$ FETs on $SiO_2$.[46] A saturation characteristic of $I_{DS}$ versus $V_{DS}$ varying from 0 to 2 V is clearly shown in Figure 2b. From the drain current vs back-gate voltage ($I_{DS}$-$V_{BG}$) transfer curves in Figures 2c and 2d, a small threshold voltage ($V_{th}$) of -0.25 V compared with the magnitude of -29.3 V for the 9.5 nm $ReS_2$ FET on 285 nm $SiO_2$ substrate (Figure S10), high current on/off ratio of ~ $10^7$ and a low *SS* of 116 mV/dec are observed at $V_{DS}$= 0.5 V, which demonstrate the good gate controllability with 20 nm-thick $HfO_2$ dielectric. Note that the gate leakage current is less than 6 *p*A in the $V_{BG}$ range of -2 to +1 V (Figure 2e). As shown in the hysteresis loop for transfer characteristics (Figure S6), the bilayer $ReS_2$ FET on $HfO_2$ with $Al_2O_3$ passivation exhibits nearly "hysteresis free" characteristics (small hysteresis of 40~50 mV at $I_{DS}$= 1 nA), which is mainly related to the reduction of surface adsorption of oxygen and water due to the passivation layer.[47] The field-effect electron mobility ( $\mu_{FE}$ ) is extracted from the linear region of the transfer curves using the following equation:

$$\mu_{FE} = \frac{\partial I_{DS}}{\partial V_G} \times \frac{L}{W C_g V_{DS}} \quad (1)$$

where $L$ and $W$ denotes the length and width of the channel, respectively, $C_g$ is the gate dielectric capacitance per unit area (F/cm$^2$), and $V_G$ is the gate voltage. Based on the derived $k$ value (15.4) of the $HfO_2$ (Figure S2), an electron mobility of 6.02 cm$^2$/V·s is obtained for the two-layer $ReS_2$ FET at $V_{DS}$ = 0.1 V. Figure 2f shows the comparison of electron mobility, on/off ratio and $SS$ for the 1.4, 4.6 and 12.7 nm-thick $ReS_2$ FETs. The output and transfer curves of the 4.6 and 12.7 nm-thick $ReS_2$ FETs on 20 nm-thick $HfO_2$ are presented in Figures S6 and S7. Higher electron mobility of 11.8 and 16.2 cm$^2$/V·s are obtained for the 4.6 nm and 12.7 nm-thick $ReS_2$ FET, respectively. These measured electron mobilities are comparable to those in $ReS_2$ FETs recently reported,[16, 46] which are summarized in Table S1. Note that though the 12.7 nm-thick $ReS_2$ FET shows a higher mobility, its current on/off ratio falls drastically to ~ 150 and the $SS$ increases to 650 mV/dec. The on/off ratio and $SS$ for our $ReS_2$ FETs on $HfO_2$ are mainly limited by the off-current passing through the inside of $ReS_2$ beneath the channel surface.[16, 48] Thicker $ReS_2$ FET shows larger "off" current and is harder to switch off, accordingly results in relatively lower on/off ratio and larger $SS$. In addition, two $ReS_2$ FETs on 285 nm-thick $SiO_2$ were also fabricated for comparison (Figure S9 and S10), and higher $SS$ of 2.6 and 4.4 V/dec are observed for the 5.3 nm-thick and 9.5 nm-thick $ReS_2$ FET, respectively. This further demonstrates the improvement of gate controllability with the use of thin $HfO_2$ gate dielectric. To study the effects of $Al_2O_3$ passivation on $ReS_2$ transistor, the electron mobility, on/off ratio, $SS$ and $V_{th}$ of a 9.5 nm-thick $ReS_2$ FET on 285 nm-thick $SiO_2$ before and after $Al_2O_3$ passivation are examined (Figure S10). It is found the $V_{th}$ shifts negatively and the $SS$ decreases, while the electron mobility and on/off ratio exhibits little change after the $Al_2O_3$ passivation.

**Noise Characteristics of $ReS_2$ FETs.** The LFN measurement is a versatile method to probe the semiconductor-insulator interface traps as well as the charge dynamics.[35] It should be noted that the drain current fluctuation of 2D FETs is sensitive to the open air ambience[38] and thus the passivation layer of $Al_2O_3$, a commonly used passivation method, ensures accurate LFN measurements in ambient. The typical power spectral densities (PSDs) of the drain current fluctuations ($S_I$) in the two-layer (1.4 nm-thick) $ReS_2$ FET as a function of frequency ($f$) at different $V_{BG}$ with constant $V_{DS} = 0.1$ V are shown in **Figure 3**a. When $V_{BG}$ = -1 V, the device is switched off, thus $S_I$ is relatively low and the PSD at high frequencies comes from the noise floor. When $V_{BG}$ is biased at 0 and 1 V, the $S_I$ follows closely a $1/f$ dependence over a wide frequency range from 1 to 1000 Hz. The $S_I$ increases with increasing $V_{BG}$ due to an increase of drain current.

To comprehend the origin of the LFN in $ReS_2$ FETs, the normalized PSD ($S_I/I_{DS}^2$) at 10 Hz as a function of the drain current is presented in Figure 3b. As can be seen, the $S_I/I_{DS}^2$ decreases with increasing $V_{BG}$ due to the increase of drain current. Two well-known models were proposed to describe the LFN in semiconducting FETs: Hooge's mobility fluctuation (HMF) resulting from the fluctuations in the mean free-path of electrons[49] and carrier number fluctuation (CNF) due to the numerous charge trapping/detrapping processes at the interface between the channel and dielectric layer.[38] As shown in Figure 3b, the normalized $S_I/I_{DS}^2$ follows the same trend of $(g_m/I_{DS})^2$, where $g_m$ is the transconductance of the transistor, which suggests the current noise behavior can be modeled by the CNF model. In addition, the CNF model can be also applied to the 4.6 nm and 12.7 nm-thick $ReS_2$ FETs (Figure S7 and S8), and the 5.3 nm-thick $ReS_2$ FET on 285 nm-thick $SiO_2$ (Figure S9). Using the CNF model,[38] the normalized current PSD can be expressed by:

$$\frac{S_I}{I_{DS}^2} = S_{Vfb}\left(\frac{g_m}{I_{DS}}\right)^2 \quad (2)$$

where $S_{Vfb} = q^2 k_B T N_{it} / fWLC_{ox}^2$ is the flat-band voltage spectral density, while $q$, $k_B$, $T$ and $N_{it}$ are the elemental charge, Boltzmann constant, absolute temperature in Kelvin, and effective trap density, respectively. The effective trap density, $N_{it}$, can be extracted from $S_{Vfb}$, which is estimated by dividing the $S_I/I_{DS}^2$ by $(g_m/I_{DS})^2$. From Figure 3b, $N_{it}$ at the interface between the channel and dielectric layers is calculated to be 8.5 × $10^{12}$ $cm^{-2}$ $eV^{-1}$ for the two-layer $ReS_2$ FET. It should be noted that the interface between the $Al_2O_3$ passivation layer and $ReS_2$ also contribute to this calculated $N_{it}$ since the conducting $ReS_2$ channel is of two atomic layer thickness and thus can be easily affected by both surrounding dielectric layers. A slightly higher $N_{it}$ of 1.62 × $10^{13}$ $cm^{-2}$ $eV^{-1}$ for the 4.6 nm-thick $ReS_2$ FET is obtained, which is consistent with its larger *SS* (144.5 mV/dec). As for the 12.7 nm-thick $ReS_2$ FET showing a higher *SS* of 650 mV/dec, its $N_{it}$ is calculated to be 4.82 × $10^{12}$ $cm^{-2}$ $eV^{-1}$ using the CNF model, which is lower than those of the 1.4 nm and 4.6 nm-thick $ReS_2$ FETs. The smaller $N_{it}$ in the 12.7 nm-thick $ReS_2$ FET could be explained as an increased distance between the top interface and the $ReS_2$ channel, which likely accumulates near the bottom interface between $ReS_2$ and $HfO_2$ under a positive back-gate bias. A similar phenomenon that the passivation of $Al_2O_3$ has little influence on $N_{it}$ for the back-gated thick (11.3 nm) $MoS_2$ FETs was also observed with the LFN.[49] In addition, Figure 3c shows the channel area multiplied normalized PSDs as a function of the overdrive voltage ($V_{BG}$-$V_{th}$). As can be seen, the FET with a thicker $ReS_2$ exhibits a lower normalized LFN.

**pH Sensing.** We further performed the pH sensing measurements of our $ReS_2$ FETs on $HfO_2$/Si. pH sensing is important in physiological and environmental monitoring applications, and is a commonly used method for examining the performance of biosensors.[29] As shown in **Figure 4**a, 20 nm-thick $HfO_2$ as the sensing layer is deposited by ALD on highly doped Si, which is wired to the back gate of $ReS_2$ FET. We chose the two-layer (1.4 nm-thick) $ReS_2$ FET for pH measurements because it exhibits a better electrostatic control than thicker channels (as shown in Figure 2f). It has also been suggested that a thin channel is required for the trace-level amount and small-size molecular detection.[36, 50]

Figure 4b shows the drain current versus the liquid gate ($V_{LG}$) at different pH values (i.e., 3.21, 4.22, 5.26 and 8.11) in both logarithmic and linear scale. The transfer curves $I_{DS}$-$V_{LG}$

shift positively with an increase in the pH value (from 3.21→4.22→5.26→8.11), which can be explained that a higher pH value in the solution causes more negative charge on the $HfO_2$ surface. Such a surface charge developed on $HfO_2$ leads to a shift of transfer curves of the transistor. The current change based sensitivity for pH sensing $S_{\text{pH-I}}$, which is commonly used for chemical sensors, is defined as the relative change of the transistor current corresponding to a unit change of the pH value, $S_{\text{pH-I}} = (I_{\text{pH1}} - I_{\text{pH2}}) / I_{\text{pH2}} \times 100$, where $I_{\text{pH1}}$ and $I_{\text{pH2}}$ are the current readings at two different pH values of the electrolyte.[36] Figure 4c compares $S_{\text{pH-I}}$ in the pH range from 4.22 to 5.26 in subthreshold, saturation and linear regions. As can be seen, $S_{\text{pH-I}}$ of 126 in the subthreshold region is significantly higher than those of 34.8 and 14.5 in the saturation and linear regions, respectively, which is due to the exponential dependence of the drain current on the gate voltage in the subthreshold regime.[29] This sensitivity $S_{\text{pH-I}}$ of 126 in the subthreshold region is significantly higher than that of 6.6 in graphene based FET biosensor[51] and comparable to the recently reported values of 196, 130, and 100 in $MoS_2$, Si nanowire, and $In_2O_3$ based FET biosensors, respectively[36, 52, 53] (Table S2). Figure 4d further demonstrates the exponential dependence of $I_{DS}$ on pH change in the subthreshold region. The shift of $V_{th}$ with different pH value (also named as a voltage sensitivity for pH sensing, $S_{\text{pH-V}}$) is estimated to be 54.8 mV/pH, a value close to the Nernstian limit of 59.2 mV/pH at room temperature. The linearity of the $V_{th}$ shift over the pH range from 3.21 to 8.11 is calculated to be 99.81%. Figure 4e shows the $I_{DS}$ as a function of time in different solutions with pH value changing from 8.11 to 3.21. The device is measured at fixed $V_{DS}$ = 0.1 V and $V_{LG}$ = −0.5 V. It is observed that the $I_{DS}$ increases stepwise with discrete changes in pH value from 8.11 to 3.21 and quickly goes to a stable value in each pH value.

The noise behavior under pH sensing was also examined to estimate the detection limit. **Figure 5**a shows the typical current PSD ($S_I$) as a function of frequency ($f$) in pH= 5.26

solution with different $V_{LG}$. The LFN shows an approximately 1/*f* characteristic. To further probe the impact of PBS solution-$HfO_2$ interface on the mechanism of current fluctuation, the normalized PSD ($S_I/I_{DS}^2$) as a function of current density under pH sensing is investigated (as shown in Figure 5b). Normalized PSD ($S_I/I_{DS}^2$) is dependent on the transconductance to drain current ratio squared $(g_m/I_{DS})^2$, and does not show a linear dependence on the $1/I_{DS}$. This suggests that the LFN in $ReS_2$ FET under pH sensing follows the CNF model, which is similar with that in dry environment. From Figure 5b, the $N_{it}$ under pH= 5.26 solution is calculated to be $8.83 \times 10^{12}$ cm$^{-2}$ eV$^{-1}$, which is close to that extrated from dry environment, suggesting that the liquid/$HfO_2$ contributes little to the overall noise. Further, the pH resolution ($\Delta pH_{Min}$),[54] which determines the smallest pH value a sensor can respond, is measured. The $\Delta pH_{Min}$ is defined as

$$\Delta \mathrm{pH}_{\mathrm{Min}} = 3\times\sqrt{S_{\mathrm{VG}}} \,/\, S_{\mathrm{pH\text{-}V}} \qquad (3)$$

where $S_{VG} = S_I / g_m^{\ 2}$ is the gate referred voltage PSD. As shown in Figure 5c, the $S_{VG}$ shows no evident dependence with pH values, which is consistent with the literature.[55, 56] The limit of detection is calculated to be 0.0132 pH at a typical sampling rate of 10 Hz with $V_{DS}$= 0.1 V and $V_{LG}$= 1 V, which is comparable with the value of 0.01 pH in APTES functionalized Si nanoribbons ion-sensitive field effect transistor (ISFET).[57]

## 3. Conclusions

Layered $ReS_2$ FETs with different thickness on 20 nm-thick high-*k* $HfO_2$ were fabricated and studied. A small threshold voltage of -0.25 V, high on/off current ratio of ~ $10^7$, low *SS* of 116 mV/dec and electron mobility of 6.02 cm$^2$/Vs are obtained for the two-layer $ReS_2$ FET. Current fluctuation in $ReS_2$ FETs is comprehensively analyzed for the first time. It is found that the CNF model dominates in the current flicker (1/*f*) noise with various $ReS_2$ channel thicknesses. pH sensing based on $ReS_2$ FETs are demonstrated with $HfO_2$ sensing layer, exhibiting a sensitivity of 54.8 mV/pH and a detection limit of 0.0132 pH. The DC, noise and pH sensing characteristics of $ReS_2$ transistor on high-*k* dielectric presented here could pave the way towards nanoelectronic devices and sensing applications.

## 4. Experimental Section

***Device Fabrication*****:** Layered $ReS_2$ flakes were obtained by micromechanical exfoliation of commercially $ReS_2$ bulk crystal (HQ graphene) and subsequently transferred onto the 20 nm-thick $HfO_2$ coated Si. Subsequently, the source/drain regions were patterned by standard electron beam lithography (EBL: JOEL-6300FS) using PMMA polymer. Cr/Au (3 nm/55 nm) were deposited by thermal evaporation which was then followed by a lift-off step. Finally, an $Al_2O_3$ layer with a thickness of 20 nm, as a passivation layer, was deposited by ALD on top of the device.

***Current-voltage and noise Measurement*****:** The current-voltage characteristics were measured in ambient on a Cascade probe station with a HP4155 semiconductor parameter analyzer. For low frequency noise measurements, the source terminal of the $ReS_2$ FETs was dc coupled to a Stanford Research SR570 low noise current preamplifier. The output of this current amplifier was recorded by a HP 35670A dynamic signal analyzer. During all the measurements, the samples were electrically shielded to avoid unwanted noise pickup.

***pH Sensing Measurement*****:** 20 nm-thick $HfO_2$ as the sensing layer is deposited by ALD on highly doped Si, which is wired to the back gate of $ReS_2$ FET. The pH sensing measurements were conducted in typical biocompatible 0.01 M solution of phosphate buffered saline (PBS) with different pH values. A silver/silver chloride (Ag/AgCl) electrode was used to set the potential of the liquid gate ($V_{LG}$).

***AFM and Raman Spectra Measurements*****:** AFM scans were conducted using a Bruker Dimension FastScan Atomic Force Microscope in the tapping mode. The Raman spectra of $ReS_2$ were measured using a WITec Raman Microscope with laser excitation at a wavelength of 532 nm. Raman light was dispersed on an 1800 groves/mm holographic grating.

**Supporting Information**

Further information on high-*k* deposition, schematic of the noise measurement, the DC and noise characterization of $ReS_2$ FETs with various thicknesses as well as performance comparison tables can be found in the **Supporting Information**.

AUTHOR INFORMATION

**Corresponding Author**

*Email: elezhucx@nus.edu.sg (C. Zhu)

**Author Contributions**

C. Z. supervised the project. W. L. performed the experiments and characterization. All authors analyzed the data, discussed the results and contributed to the final manuscript.

**Notes**

The authors declare no competing financial interest.

ACKNOWLEDGMENTS

This work was supported by the Singapore A☆STAR Science and Engineering Research Council Grant (No. R-263-000-B89-305). Authors acknowledge the technical support from Centre for Advanced 2D Materials and Graphene Research Centre for the device fabrication.

**REFERENCES**

(1) Novoselov, K. S.; Geim, A. K.; Morozov, S. V.; Jiang, D.; Zhang, Y.; Dubonos, S. V.; Grigorieva, I. V.; Firsov, A. A. Electric Field Effect in Atomically Thin Carbon Films. *Science* **2004,** 306(5696), 666-669.

(2) Lin, Z.; McCreary, A.; Briggs, N.; Subramanian, S.; Zhang, K.; Sun, Y.; Li, X.; Borys, N. J.; Yuan, H.; Fullerton-Shirey, S. K.; Chernikov, A.; Zhao, H.; McDonnell, S.; Lindenberg, A. M.; Xiao, K.; LeRoy, B. J.; Drndić, M.; Hwang, J. C. M.; Park, J.; Chhowalla, M.; Schaak, R. E.; Javey, A.; Hersam, M. C.; Robinson, J.; Terrones, M. 2D Materials Advances: From Large Scale Synthesis and Controlled Heterostructures to Improved Characterization Techniques, Defects and Applications. *2D Materials* **2016,** 3(4), 042001.

(3) Kannan, P. K.; Late, D. J.; Morgan, H.; Rout, C. S. Recent Developments in 2D Layered Inorganic Nanomaterials for Sensing. *Nanoscale* **2015,** 7(32), 13293-13312.

(4) Late, D. J.; Huang, Y.-K.; Liu, B.; Acharya, J.; Shirodkar, S. N.; Luo, J.; Yan, A.; Charles, D.; Waghmare, U. V.; Dravid, V. P. Sensing Behavior of Atomically Thin-Layered $MoS_2$ Transistors. *ACS Nano* **2013,** 7(6), 4879-4891.

(5) Fiori, G.; Bonaccorso, F.; Iannaccone, G.; Palacios, T.; Neumaier, D.; Seabaugh, A.; Banerjee, S. K.; Colombo, L. Electronics Based on Two-Dimensional Materials. *Nat. Nanotechnol.* **2014,** 9(10), 768-779.

(6) Yu, L.; Zubair, A.; Santos, E. J.; Zhang, X.; Lin, Y.; Zhang, Y.; Palacios, T. High-Performance $WSe_2$ Complementary Metal Oxide Semiconductor Technology and Integrated Circuits. *Nano Lett.* **2015,** 15(8), 4928-4934.

(7) Choi, W.; Choudhary, N.; Han, G. H.; Park, J.; Akinwande, D.; Lee, Y. H. Recent Development of Two-Dimensional Transition Metal Dichalcogenides and Their Applications. *Mater. Today* **2017,** 20(3), 116-130.

(8) Pawbake, A. S.; Waykar, R. G.; Late, D. J.; Jadkar, S. R. Highly Transparent Wafer-Scale Synthesis of Crystalline $WS_2$ Nanoparticle Thin Film for Photodetector and Humidity-Sensing

Applications. *ACS Appl. Mater. Inter.* **2016,** 8(5), 3359-3365.

(9) Late, D. J.; Doneux, T.; Bougouma, M. Single-Layer $MoSe_2$ Based $NH_3$ Gas Sensor. *Appl. Phys. Lett.* **2014,** 105(23), 233103.

(10) Jariwala, D.; Sangwan, V. K.; Late, D. J.; Johns, J. E.; Dravid, V. P.; Marks, T. J.; Lauhon, L. J.; Hersam, M. C. Band-Like Transport in High Mobility Unencapsulated Single-Layer $MoS_2$ Transistors. *Appl. Phys. Lett.* **2013,** 102(17), 173107.

(11) Erande, M. B.; Pawar, M. S.; Late, D. J. Humidity Sensing and Photodetection Behavior of Electrochemically Exfoliated Atomically Thin-Layered Black Phosphorus Nanosheets. *ACS Appl. Mater. Inter.* **2016,** 8(18), 11548-11556.

(12) Liu, E.; Fu, Y.; Wang, Y.; Feng, Y.; Liu, H.; Wan, X.; Zhou, W.; Wang, B.; Shao, L.; Ho, C. H.; Huang, Y. S.; Cao, Z.; Wang, L.; Li, A.; Zeng, J.; Song, F.; Wang, X.; Shi, Y.; Yuan, H.; Hwang, H. Y.; Cui, Y.; Miao, F.; Xing, D. Integrated Digital Inverters Based on Two-Dimensional Anisotropic $ReS_2$ Field-Effect Transistors. *Nat. Commun.* **2015,** 6, 6991.

(13) Tian, H.; Tice, J.; Fei, R.; Tran, V.; Yan, X.; Yang, L.; Wang, H. Low-Symmetry Two-Dimensional Materials for Electronic and Photonic Applications. *Nano Today* **2016,** 11(6), 763-777.

(14) Chenet, D. A.; Aslan, O. B.; Huang, P. Y.; Fan, C.; van der Zande, A. M.; Heinz, T. F.; Hone, J. C. In-Plane Anisotropy in Mono- and Few-Layer $ReS_2$ Probed by Raman Spectroscopy and Scanning Transmission Electron Microscopy. *Nano Lett.* **2015,** 15(9), 5667-5672.

(15) Aslan, O. B.; Chenet, D. A.; van der Zande, A. M.; Hone, J. C.; Heinz, T. F. Linearly Polarized Excitons in Single- and Few-Layer $ReS_2$ Crystals. *ACS Photonics* **2016,** 3(1), 96-101.

(16) Shim, J.; Oh, A.; Kang, D. H.; Oh, S.; Jang, S. K.; Jeon, J.; Jeon, M. H.; Kim, M.; Choi, C.; Lee, J.; Lee, S.; Yeom, G. Y.; Song, Y. J.; Park, J. H. High-Performance 2D Rhenium Disulfide ($ReS_2$) Transistors and Photodetectors by Oxygen Plasma Treatment. *Adv. Mater.*

**2016,** 28(32), 6985-6992.

(17) Liu, E.; Long, M.; Zeng, J.; Luo, W.; Wang, Y.; Pan, Y.; Zhou, W.; Wang, B.; Hu, W.; Ni, Z.; You, Y.; Zhang, X.; Qin, S.; Shi, Y.; Watanabe, K.; Taniguchi, T.; Yuan, H.; Hwang, H. Y.; Cui, Y.; Miao, F.; Xing, D. High Responsivity Phototransistors Based on Few-Layer $ReS_2$ for Weak Signal Detection. *Adv. Funct. Mater.* **2016,** 26(12), 1938-1944.

(18) Yang, S.; Kang, J.; Yue, Q.; Coey, J. M. D.; Jiang, C. Defect-Modulated Transistors and Gas-Enhanced Photodetectors on $ReS_2$ Nanosheets. *Adv. Mater. Interfaces* **2016,** 3(6), 1500707.

(19) He, R.; Yan, J. A.; Yin, Z.; Ye, Z.; Ye, G.; Cheng, J.; Li, J.; Lui, C. H. Coupling and Stacking Order of $ReS_2$ Atomic Layers Revealed by Ultralow-Frequency Raman Spectroscopy. *Nano Lett.* **2016,** 16(2), 1404-1409.

(20) Zhang, E.; Jin, Y.; Yuan, X.; Wang, W.; Zhang, C.; Tang, L.; Liu, S.; Zhou, P.; Hu, W.; Xiu, F. $ReS_2$-Based Field-Effect Transistors and Photodetectors. *Adv. Funct. Mater.* **2015,** 25(26), 4076-4082.

(21) Dathbun, A.; Kim, Y.; Kim, S.; Yoo, Y.; Kang, M. S.; Lee, C.; Cho, J. H. Large-Area CVD-Grown Sub-2 V $ReS_2$ Transistors and Logic Gates. *Nano Lett.* **2017,** 17(5), 2999-3005.

(22) Gutiérrez-Lezama, I.; Reddy, B. A.; Ubrig, N.; Morpurgo, A. F. Electroluminescence from Indirect Band Gap Semiconductor $ReS_2$. *2D Materials* **2016,** 3(4), 045016.

(23) Ganapathi, K. L.; Bhattacharjee, S.; Mohan, S.; Bhat, N. High-Performance $HfO_2$ Back Gated Multilayer $MoS_2$ Transistors. *IEEE Electron Device Lett.* **2016,** 37(6), 797-800.

(24) Xu, J.; Chen, L.; Dai, Y.-W.; Cao, Q.; Sun, Q.-Q.; Ding, S.-J.; Zhu, H.; Zhang, D. W. A Two-Dimensional Semiconductor Transistor with Boosted Gate Control and Sensing Ability. *Sci. Adv.* **2017,** 3(5), e1602246.

(25) Li, X.; Yang, L.; Si, M.; Li, S.; Huang, M.; Ye, P.; Wu, Y. Performance Potential and Limit of $MoS_2$ Transistors. *Adv. Mater.* **2015,** 27(9), 1547-1552.

(26) Xie, X.; Sarkar, D.; Liu, W.; Kang, J.; Marinov, O.; Deen, M. J.; Banerjee, K. Low-

Frequency Noise in Bilayer $MoS_2$ Transistor. *ACS Nano* **2014,** 8(6), 5633-5640.

(27) Sangwan, V. K.; Arnold, H. N.; Jariwala, D.; Marks, T. J.; Lauhon, L. J.; Hersam, M. C. Low-Frequency Electronic Noise in Single-Layer $MoS_2$ Transistors. *Nano Lett.* **2013,** 13(9), 4351-4355.

(28) Ishigami, M.; Chen, J. H.; Williams, E. D.; Tobias, D.; Chen, Y. F.; Fuhrer, M. S. Hooge's Constant for Carbon Nanotube Field Effect Transistors. *Appl. Phys. Lett.* **2006,** 88(20), 203116.

(29) Wu, T.; Alharbi, A.; You, K.-D.; Kisslinger, K.; Stach, E. A.; Shahrjerdi, D. Experimental Study of the Detection Limit in Dual-Gate Biosensors Using Ultra-Thin Silicon Transistors. *ACS Nano* **2017,** 11(7), 7142-7147.

(30) Stolyarov, M. A.; Liu, G.; Rumyantsev, S. L.; Shur, M.; Balandin, A. A. Suppression of 1/f Noise in near-Ballistic h-BN-Graphene-h-BN Heterostructure Field-Effect Transistors. *Appl. Phys. Lett.* **2015,** 107(2), 023106.

(31) Ji, H.; Joo, M.-K.; Yun, Y.; Park, J.-H.; Lee, G.; Moon, B. H.; Yi, H.; Suh, D.; Lim, S. C. Suppression of Interfacial Current Fluctuation in $MoTe_2$ Transistors with Different Dielectrics. *ACS Appl. Mater. Inter.* **2016,** 8(29), 19092-19099.

(32) Das, S. R.; Kwon, J.; Prakash, A.; Delker, C. J.; Das, S.; Janes, D. B. Low-Frequency Noise in $MoSe_2$ Field Effect Transistors. *Appl. Phys. Lett.* **2015,** 106(8), 083507.

(33) Cho, I.-T.; Kim, J. I.; Hong, Y.; Roh, J.; Shin, H.; Baek, G. W.; Lee, C.; Hong, B. H.; Jin, S. H.; Lee, J.-H. Low Frequency Noise Characteristics in Multilayer $WSe_2$ Field Effect Transistor. *Appl. Phys. Lett.* **2015,** 106(2), 023504.

(34) Rumyantsev, S. L.; Jiang, C.; Samnakay, R.; Shur, M. S.; Balandin, A. A. 1/f Noise Characteristics of $MoS_2$ Thin-Film Transistors: Comparison of Single and Multilayer Structures. *IEEE Electron Device Lett.* **2015,** 36(5), 517-519.

(35) Kumar, C.; Kuiri, M.; Jung, J.; Das, T.; Das, A. Tunability of 1/f Noise at Multiple Dirac Cones in hBN Encapsulated Graphene Devices. *Nano Lett.* **2016,** 16(2), 1042-1049.

(36) Sarkar, D.; Liu, W.; Xie, X.; Anselmo, A. C.; Mitragotri, S.; Banerjee, K. $MoS_2$ Field-Effect Transistor for Next-Generation Label-Free Biosensors. *ACS Nano* **2014,** 8(4), 3992-4003.

(37) Balandin, A. A. Low-Frequency 1/f Noise in Graphene Devices. *Nat. Nanotechnol.* **2013,** 8(8), 549-555.

(38) Lin, Y. F.; Xu, Y.; Lin, C. Y.; Suen, Y. W.; Yamamoto, M.; Nakaharai, S.; Ueno, K.; Tsukagoshi, K. Origin of Noise in Layered $MoTe_2$ Transistors and Its Possible Use for Environmental Sensors. *Adv. Mater.* **2015,** 27(42), 6612-6619.

(39) Liao, W.; Wei, W.; Tong, Y.; Chim, W. K.; Zhu, C. Electrical Performance and Low Frequency Noise in Hexagonal Boron Nitride Encapsulated $MoSe_2$ Dual-Gated Field Effect Transistors. *Appl. Phys. Lett.* **2017,** 111(8), 082105.

(40) Liu, F.; Zheng, S.; He, X.; Chaturvedi, A.; He, J.; Chow, W. L.; Mion, T. R.; Wang, X.; Zhou, J.; Fu, Q.; Fan, H. J.; Tay, B. K.; Song, L.; He, R.-H.; Kloc, C.; Ajayan, P. M.; Liu, Z. Highly Sensitive Detection of Polarized Light Using Anisotropic 2D $ReS_2$. *Adv. Funct. Mater.* **2016,** 26(8), 1169-1177.

(41) Shim, J.; Oh, S.; Kang, D. H.; Jo, S. H.; Ali, M. H.; Choi, W. Y.; Heo, K.; Jeon, J.; Lee, S.; Kim, M.; Song, Y. J.; Park, J. H. Phosphorene/Rhenium Disulfide Heterojunction-Based Negative Differential Resistance Device for Multi-Valued Logic. *Nat. Commun.* **2016,** 7, 13413.

(42) Keyshar, K.; Gong, Y.; Ye, G.; Brunetto, G.; Zhou, W.; Cole, D. P.; Hackenberg, K.; He, Y.; Machado, L.; Kabbani, M.; Hart, A. H.; Li, B.; Galvao, D. S.; George, A.; Vajtai, R.; Tiwary, C. S.; Ajayan, P. M. Chemical Vapor Deposition of Monolayer Rhenium Disulfide ($ReS_2$). *Adv. Mater.* **2015,** 27(31), 4640-4648.

(43) Jariwala, B.; Voiry, D.; Jindal, A.; Chalke, B. A.; Bapat, R.; Thamizhavel, A.; Chhowalla, M.; Deshmukh, M.; Bhattacharya, A. Synthesis and Characterization of $ReS_2$ and $ReSe_2$ Layered Chalcogenide Single Crystals. *Chem. Mater.* **2016,** 28(10), 3352-3359.

(44) Chang, H.-Y.; Zhu, W.; Akinwande, D. On the Mobility and Contact Resistance Evaluation for Transistors Based on $MoS_2$ or Two-Dimensional Semiconducting Atomic Crystals. *Appl. Phys. Lett.* **2014,** 104(11), 113504.

(45) Xu, Y.; Minari, T.; Tsukagoshi, K.; Chroboczek, J. A.; Ghibaudo, G. Direct Evaluation of Low-Field Mobility and Access Resistance in Pentacene Field-Effect Transistors. *J. Appl. Phys.* **2010,** 107(11), 114507.

(46) Corbet, C. M.; McClellan, C.; Rai, A.; Sonde, S. S.; Tutuc, E.; Banerjee, S. K. Field Effect Transistors with Current Saturation and Voltage Gain in Ultrathin $ReS_2$. *ACS Nano* **2014,** 9(1), 363-370.

(47) Late, D. J.; Liu, B.; Matte, H. R.; Dravid, V. P.; Rao, C. Hysteresis in Single-Layer $MoS_2$ Field Effect Transistors. *ACS Nano* **2012,** 6(6), 5635-5641.

(48) Zhang, Y.; Ye, J.; Matsuhashi, Y.; Iwasa, Y. Ambipolar $MoS_2$ Thin Flake Transistors. *Nano Lett.* **2012,** 12(3), 1136-1140.

(49) Na, J.; Joo, M. K.; Shin, M.; Huh, J.; Kim, J. S.; Piao, M.; Jin, J. E.; Jang, H. K.; Choi, H. J.; Shim, J. H.; Kim, G. T. Low-Frequency Noise in Multilayer $MoS_2$ Field-Effect Transistors: The Effect of High-k Passivation. *Nanoscale* **2014,** 6(1), 433-441.

(50) Nam, H.; Oh, B. R.; Chen, P.; Chen, M.; Wi, S.; Wan, W.; Kurabayashi, K.; Liang, X. Multiple $MoS_2$ Transistors for Sensing Molecule Interaction Kinetics. *Sci. Rep.* **2015,** 5, 10546.

(51) Li, H.; Zhu, Y.; Islam, M. S.; Rahman, M. A.; Walsh, K. B.; Koley, G. Graphene Field Effect Transistors for Highly Sensitive and Selective Detection of $K^+$ Ions. *Sensors Actuators B: Chem.* **2017,** 253, 759-765.

(52) Chen, H.; Rim, Y. S.; Wang, I. C.; Li, C.; Zhu, B.; Sun, M.; Goorsky, M. S.; He, X.; Yang, Y. Quasi-Two-Dimensional Metal Oxide Semiconductors Based Ultrasensitive Potentiometric Biosensors. *ACS Nano* **2017,** 11(5), 4710-4718.

(53) Gao, X. P.; Zheng, G.; Lieber, C. M. Subthreshold Regime Has the Optimal Sensitivity

for Nanowire FET Biosensors. *Nano Lett.* **2010,** 10(2), 547-552.

(54) Go, J.; Nair, P. R.; Alam, M. A. Theory of Signal and Noise in Double-Gated Nanoscale Electronic pH Sensors. *J. Appl. Phys.* **2012,** 112(3), 34516.

(55) Kaisti, M. Detection Principles of Biological and Chemical FET Sensors. *Biosens. Bioelectron.* **2017,** 98, 437-448.

(56) Jakobson, C.; Nemirovsky, Y. 1/f Noise in Ion Sensitive Field Effect Transistors from Subthreshold to Saturation. *IEEE Trans. Electron Devices* **1999,** 46(1), 259-261.

(57) Rajan, N. K.; Brower, K.; Duan, X.; Reed, M. A. Limit of Detection of Field Effect Transistor Biosensors: Effects of Surface Modification and Size Dependence. *Appl. Phys. Lett.* **2014,** 104(8), 084106.

## Figure Captions:

Figure 1: (a) Sketch of the $ReS_2$ FET on 20 nm $HfO_2$/Si substrate. A layer of 20 nm $Al_2O_3$ on top of the device is used as the passivation layer. (b) An optical image of a pair of Cr/Au electrodes deposited on two-layer $ReS_2$ flake. The length and width of the $ReS_2$ channel is 1.72 μm, and 3.01 μm, respectively. The scale bar is 10 μm. (c) AFM image of the two-layer $ReS_2$ FETs on $HfO_2$. (d) Measured height at the flake edge of $ReS_2$ flake. (e) Raman spectrum of the two-layer $ReS_2$ flake.

Figure 2. (a) $I_{DS}$ as a function of $V_{DS}$ ranging from -0.2 to 0.2 V with the $V_{BG}$ varying from -2 to 1 V in steps of 0.5 V. (b) $I_{DS}$ as a function of $V_{DS}$ ranging from 0 to 2 V with $V_{BG}$ varying from -2 to 1 V in steps of 0.5 V, showing the linear and saturation region. (c) $I_{DS}$ versus $V_{BG}$ with fixed $V_{DS}$ at 0.01, 0.1 and 0.5 V plotted in logarithmic scale. (d) $I_{DS}$ versus $V_{BG}$ with fixed $V_{DS}$ at 0.01, 0.1 and 0.5 V plotted in linear scale. The inset is the $I_{DS}$-$V_{BG}$ curve at $V_{DS}$ = 0.5 V, showing $V_{th}$ of -0.25 V. (e) The gate leakage as a function of the $V_{BG}$ with $V_{DS}$ at 0.01, 0.1 and 0.5 V. The total contact pad area is $6 \times 10^4$ $\mu m^2$. Plots (a) to (e) are for the 1.4 nm-thick $ReS_2$ FET. (f) Comparison of the on/off current ratio, *SS*, and electron mobility for the 1.4, 4.6 and 12.7 nm $ReS_2$ FETs.

Figure 3. (a) Typical $S_I$ as a function of frequency with different $V_{BG}$. The value of $V_{DS}$ is kept at 0.1 V. The dashed line indicates the slope of 1/*f*. (b) Normalized PSD ($S_I/I_{DS}^2$) and a constant $\times(g_m/I_{DS})^2$ as a function of $I_{DS}$. The dotted line indicates the slope of $1/I_{DS}$. Plots (a) and (b) are for the 1.4 nm-thick $ReS_2$ FET. (c) Normalized PSDs (@10 Hz) multiplied by the device area (*WL*) for the 1.4, 4.6 and 12.7 nm $ReS_2$ FETs as a function of the gate overdrive voltage ($V_{BG}$-$V_{th}$). The $V_{DS}$ is fixed at 0.1 V.

Figure 4. (a) A schematic diagram of a $ReS_2$ FET for pH sensing. A Ag/AgCl electrode is used as the liquid gate. A poly(dimethylsiloxane) (PDMS) reservoir with size of 0.6 × 0.4× 0.4 mm (Length × Width × Height) is glued onto the $HfO_2$ by epoxy to hold the PBS solutions. (b) Transfer curves ($I_{DS}$-$V_{LG}$) at different pH values (3.21, 4.22, 5.26 and 8.11) in both logarithmic and linear scale. The $V_{DS}$ is kept at 0.1 V. (c) Sensitivity ($S_{pH\text{-}I}$) in subthreshold, saturation and linear regions for a pH change from 4.22 to 5.26 calculated from the transfer curves shown in (b). (d) The shift of the $V_{th}$ and change of the $I_{DS}$ of $ReS_2$ FET as a function pH value. (e) Response curve for pH sensing with $V_{DS}$= 0.1 V and $V_{LG}$= -0.5 V at room temperature. Plots (b) to (e) are for the 1.4 nm-thick $ReS_2$ FET.

Figure 5. (a) The typical $S_I$ as a function of frequency (*f*) in pH= 5.26 PBS solution with different $V_{LG}$. The $V_{DS}$ is kept at 0.1 V. (b) $S_I/I_{DS}^2$ and a constant $\times(g_m/I_{DS})^2$ as a function of $I_{DS}$ (in pH= 5.26 solution). The dotted line indicates the slope of $1/I_{DS}$. (c) Voltage PSD ($S_{VG}$) as a function of frequency (*f*) in PBS solution with different pH values at $V_{LG}$= 1V and $V_{DS}$= 0.1 V. Plots (a) to (c) are for the 1.4 nm-thick $ReS_2$ FET.

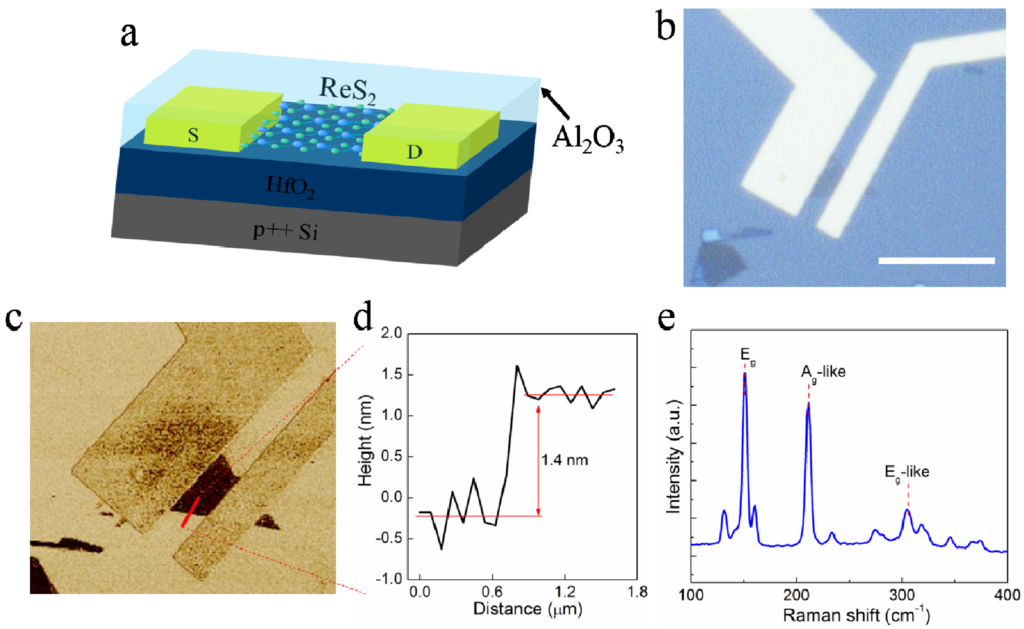
a
ReS2
S
D
Al2O3
HfO2
p++ Si
b
c
d
Height (nm)
Distance (μm)
1.4 nm
e
Eg
Ag-like
Eg-like
Intensity (a.u.)
Raman shift (cm-1)

Figure 1.

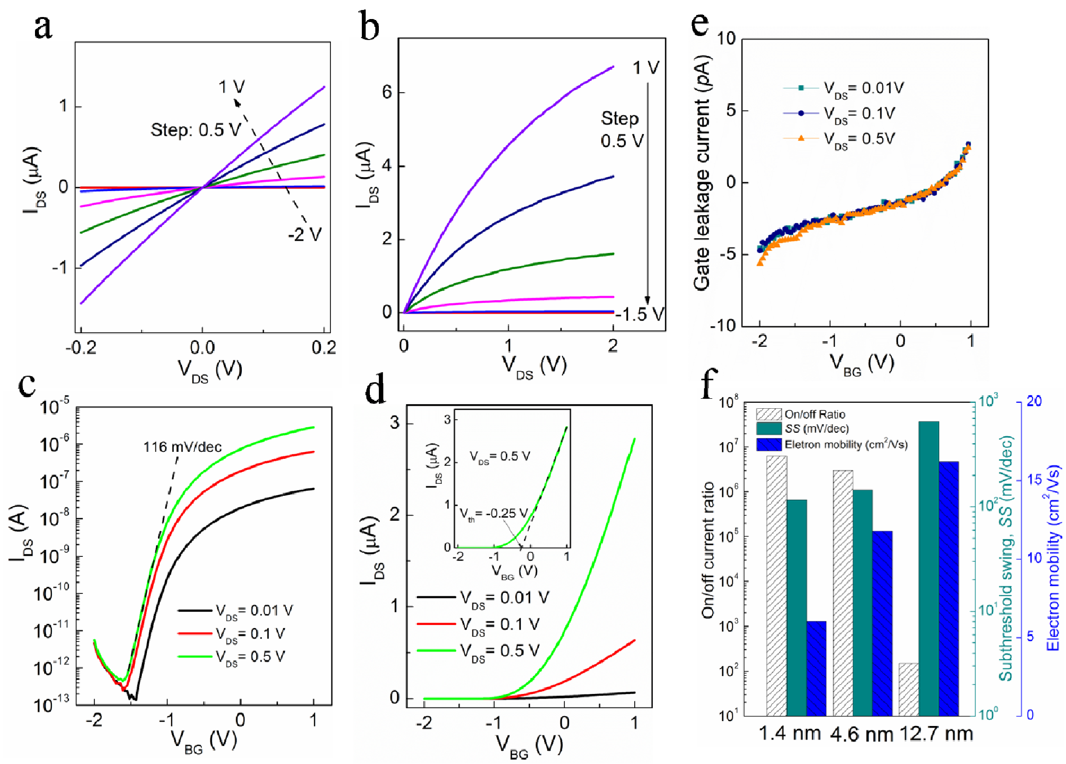
a
1 V
Step: 0.5 V
-2 V
$I_{DS}$ (μA)
$V_{DS}$ (V)
b
1 V
Step 0.5 V
-1.5 V
$I_{DS}$ (μA)
$V_{DS}$ (V)
e
$V_{DS}$= 0.01V
$V_{DS}$= 0.1V
$V_{DS}$= 0.5V
Gate leakage current (pA)
$V_{BG}$ (V)
c
116 mV/dec
$V_{DS}$= 0.01 V
$V_{DS}$= 0.1 V
$V_{DS}$= 0.5 V
$I_{DS}$ (A)
$V_{BG}$ (V)
d
$V_{DS}$= 0.5 V
$V_{th}$= -0.25 V
$V_{DS}$= 0.01 V
$V_{DS}$= 0.1 V
$V_{DS}$= 0.5 V
$I_{DS}$ (μA)
$V_{BG}$ (V)
f
On/off Ratio
SS (mV/dec)
Eletron mobility (cm²/Vs)
On/off current ratio
Subthreshold swing, SS (mV/dec)
Electron mobility (cm²/Vs)
1.4 nm 4.6 nm 12.7 nm

Figure 2.

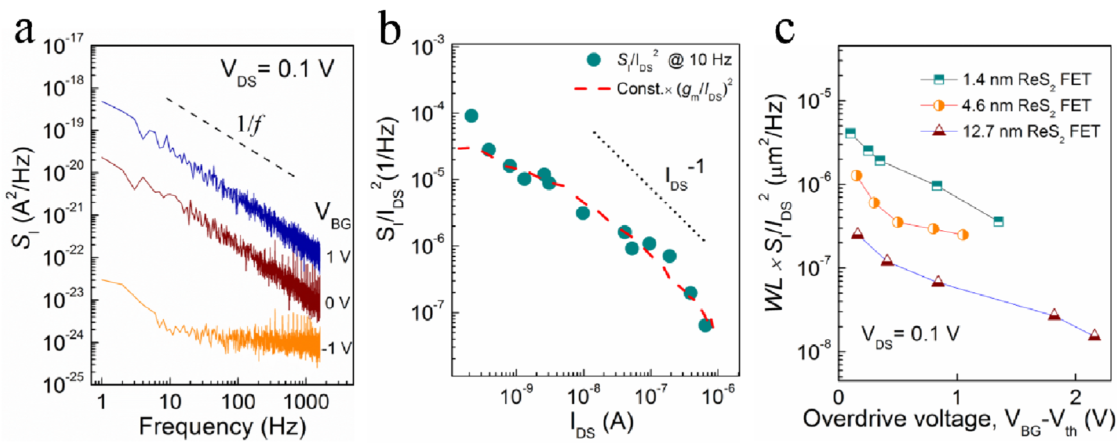
a
$V_{DS}$= 0.1 V
1/f
$V_{BG}$
1 V
0 V
-1 V
$S_I$ ($A^2$/Hz)
Frequency (Hz)
b
$S_I/I_{DS}^2$ @ 10 Hz
Const.× $(g_m/I_{DS})^2$
$I_{DS}^{-1}$
$S_I/I_{DS}^2$(1/Hz)
$I_{DS}$ (A)
c
1.4 nm $ReS_2$ FET
4.6 nm $ReS_2$ FET
12.7 nm $ReS_2$ FET
$V_{DS}$= 0.1 V
$WL \times S_I/I_{DS}^2$ ($\mu m^2$/Hz)
Overdrive voltage, $V_{BG}$-$V_{th}$ (V)

Figure 3.

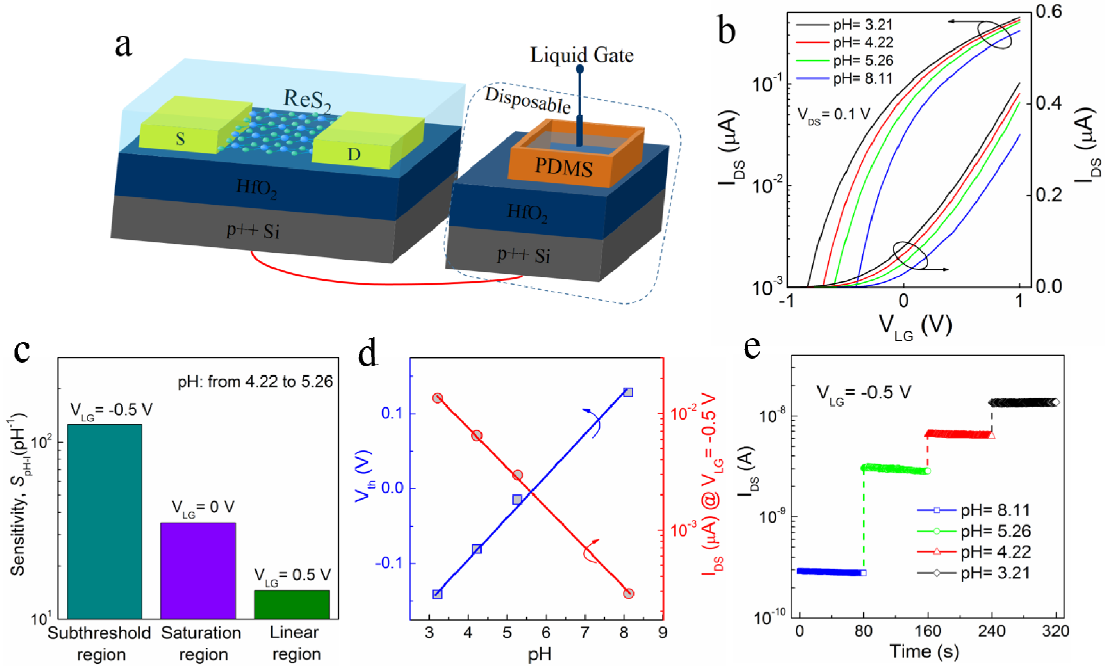
a
Liquid Gate
ReS2
Disposable
S
D
PDMS
HfO2
HfO2
p++ Si
p++ Si
b
pH= 3.21
pH= 4.22
pH= 5.26
pH= 8.11
VDS= 0.1 V
IDS (μA)
VLG (V)
c
pH: from 4.22 to 5.26
VLG= -0.5 V
VLG= 0 V
VLG= 0.5 V
Sensitivity, SpH-I(pH-1)
Subthreshold region
Saturation region
Linear region
d
Vth (V)
IDS (μA) @ VLG = -0.5 V
pH
e
VLG= -0.5 V
IDS (A)
pH= 8.11
pH= 5.26
pH= 4.22
pH= 3.21
Time (s)

Figure 4.

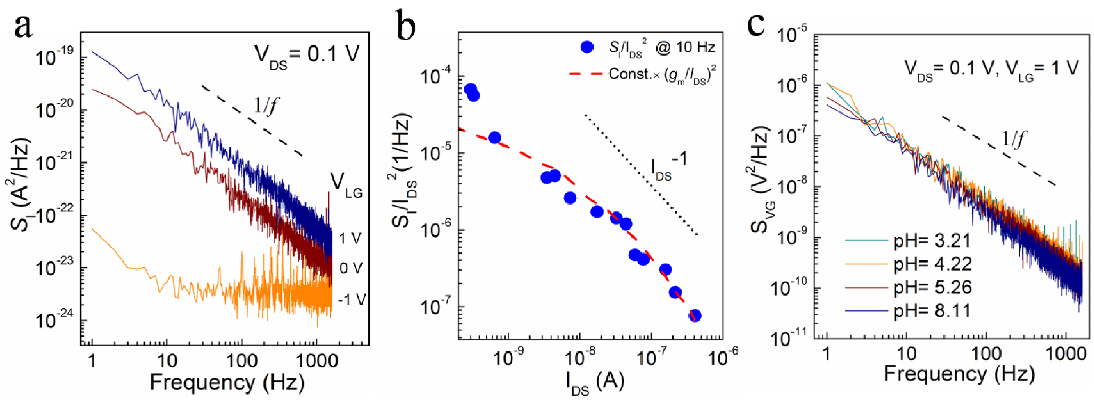
a
$V_{DS}$= 0.1 V
1/f
$V_{LG}$
1 V
0 V
-1 V
$S_I$ ($A^2$/Hz)
Frequency (Hz)
b
$S_I/I_{DS}^2$ @ 10 Hz
Const.× $(g_m/I_{DS})^2$
$I_{DS}^{-1}$
$S_I/I_{DS}^2$(1/Hz)
$I_{DS}$ (A)
c
$V_{DS}$= 0.1 V, $V_{LG}$= 1 V
1/f
pH= 3.21
pH= 4.22
pH= 5.26
pH= 8.11
$S_{VG}$ ($V^2$/Hz)
Frequency (Hz)

Figure 5.

**TOC:**

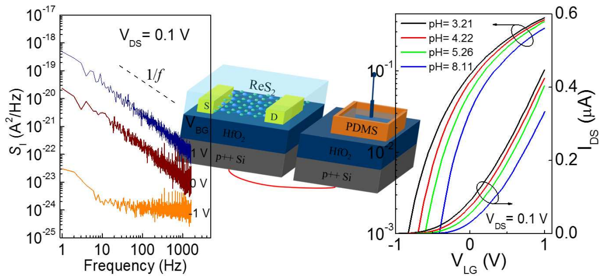
V_DS = 0.1 V
1/f
S_I (A²/Hz)
Frequency (Hz)
ReS₂
S
D
HfO₂
p++ Si
PDMS
pH= 3.21
pH= 4.22
pH= 5.26
pH= 8.11
I_DS (μA)
V_LG (V)
V_DS = 0.1 V